Elucidation of Conformational States, Dynamics, and Mechanism of Binding in Human κ-Opioid Receptor Complexes

ARTICLE *in* JOURNAL OF CHEMICAL INFORMATION AND MODELING · JULY 2014

Impact Factor: 3.74 · DOI: 10.1021/ci5002873 · Source: PubMed

6 AUTHORS, INCLUDING:

Georgios Leonis
National Hellenic Research Foundation
22 PUBLICATIONS **83** CITATIONS
SEE PROFILE

Aggelos Avramopoulos
National Hellenic Research Foundation
51 PUBLICATIONS **544** CITATIONS
SEE PROFILE

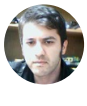

Ramin Ekhteiari Salmas
Istanbul Technical University
18 PUBLICATIONS **20** CITATIONS
SEE PROFILE

Serdar Durdagi
Bahçeşehir University
81 PUBLICATIONS **817** CITATIONS
SEE PROFILE

JOURNAL OF CHEMICAL INFORMATION AND MODELING

Article

pubs.acs.org/jcim

Elucidation of Conformational States, Dynamics, and Mechanism of Binding in Human κ-Opioid Receptor Complexes

Georgios Leonis,*[,†] Aggelos Avramopoulos,[†] Ramin Ekhteiari Salmas,[‡] Serdar Durdagi,[§] Mine Yurtsever,[‡] and Manthos G. Papadopoulos*[,†]

[†]Institute of Biology, Medicinal Chemistry and Biotechnology, National Hellenic Research Foundation, 48 Vas. Constantinou Avenue, Athens, Attiki 11635, Greece

[‡]Department of Chemistry, Istanbul Technical University, Istanbul, Istanbul 34469, Turkey

[§]Department of Biophysics, School of Medicine, Bahcesehir University, Istanbul, Istanbul 34349, Turkey

Supporting Information

ABSTRACT: Opioid G protein-coupled receptors (GPCRs) have been implicated in modulating pain, addiction, psychotomimesis, mood and memory, among other functions. We have employed the recently reported crystal structure of the human κ-opioid receptor (κ-OR) and performed molecular dynamics (MD), free energy, and *ab initio* calculations to elucidate the binding mechanism in complexes with antagonist JDTic and agonist SalA. The two systems were modeled in water and in DPPC lipid bilayers, in order to investigate the effect of the membrane upon conformational dynamics. MD and Atoms in Molecules (AIM) *ab initio* calculations for the complexes in water showed that each ligand was stabilized inside the binding site of the receptor through hydrogen bond interactions that involved residues Asp138 (with JDTic) and Gln115, His291, Leu212 (with SalA). The static description offered by the crystal structure was overcome to reveal a structural rearrangement of the binding pocket, which facilitated additional interactions between JDTic and Glu209/Tyr139. The role of Glu209 was emphasized, since it belongs to an extracellular loop that covers the binding site of the receptor and is crucial for ligand entrapment. The above interactions were retained in membrane complexes (SalA forms additional hydrogen bonds with Tyr139/312), except the Tyr139 interaction, which is abolished in the JDTic complex. For the first time, we report that JDTic alternates between a "V-shape" (stabilized via a water-mediated intramolecular interaction) and a more extended conformation, a feature that offers enough suppleness for effective binding. Moreover, MM−PBSA calculations showed that the more efficient JDTic binding to κ-OR compared to SalA (ΔG_{JDTic} = −31.6 kcal mol^{-1}, ΔG_{SalA} = −9.8 kcal mol^{-1}) is attributed mostly to differences in electrostatic contributions. Importantly, our results are in qualitative agreement with the experiments ($\Delta G_{JDTic,exp}$ = −14.4 kcal mol^{-1}, $\Delta G_{SalA,exp}$ = −10.8 kcal mol^{-1}). This study provides previously unattainable information on the dynamics of human κ-OR and insight on the rational design of drugs with improved pharmacological properties.

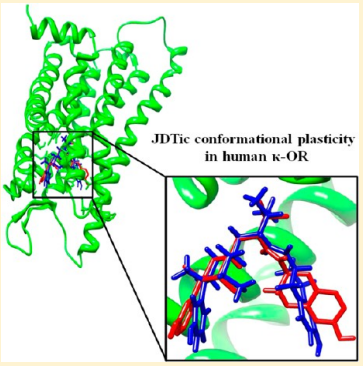

I. INTRODUCTION

G protein-coupled receptors (GPCRs) are the most common family of proteins involved in transmitting signals into cells.[1,2] These receptors enable the cells to sense external signals (e.g., taste, pain) or to communicate with each other via messenger molecules. They are implicated in a variety of physiological processes and are targeted by ∼40% of current prescription drugs.[3]

Despite consistent efforts over the years, the solution of GPCRs structures remains a great challenge: GPCR incorporation into a membrane is a prerequisite for retaining the protein's structural integrity; however, it is hardly achieved experimentally. Additionally, the high flexibility of several loop regions renders their expression arduous. Nevertheless, major progress has been made recently, as several crystal structures were obtained and helped considerably toward understanding of GPCR structure and action.[4−13]

All of the structures solved so far confirm that GPCRs are integral membrane proteins with seven α-helical membrane-spanning regions. These regions are linked together via three extracellular and three intracellular loops to define a common overall architecture for GPCRs. Opioid (μ, δ, κ, and nociceptin) receptors (ORs) belong to the class A (rhodopsin-like) γ subfamily of GPCRs.[14] Activation of these receptors is associated with a multitude of neuropsychiatric responses (e.g., depression, schizophrenia, analgesia, euphoria) and physiological processes, including memory and learning.[15] The κ-OR subtype represents an excellent model for drug design, since numerous κ-OR−selective agonists/antagonists have been developed as compounds with antiaddictive, antidepressant, and anxiolytic action.[16] Salvinorin A (SalA), which is the active ingredient of the hallucinogenic plant *Salvia*

Received: May 13, 2014

   dx.doi.org/10.1021/ci5002873 | *J. Chem. Inf. Model.* XXXX, XXX, XXX−XXX

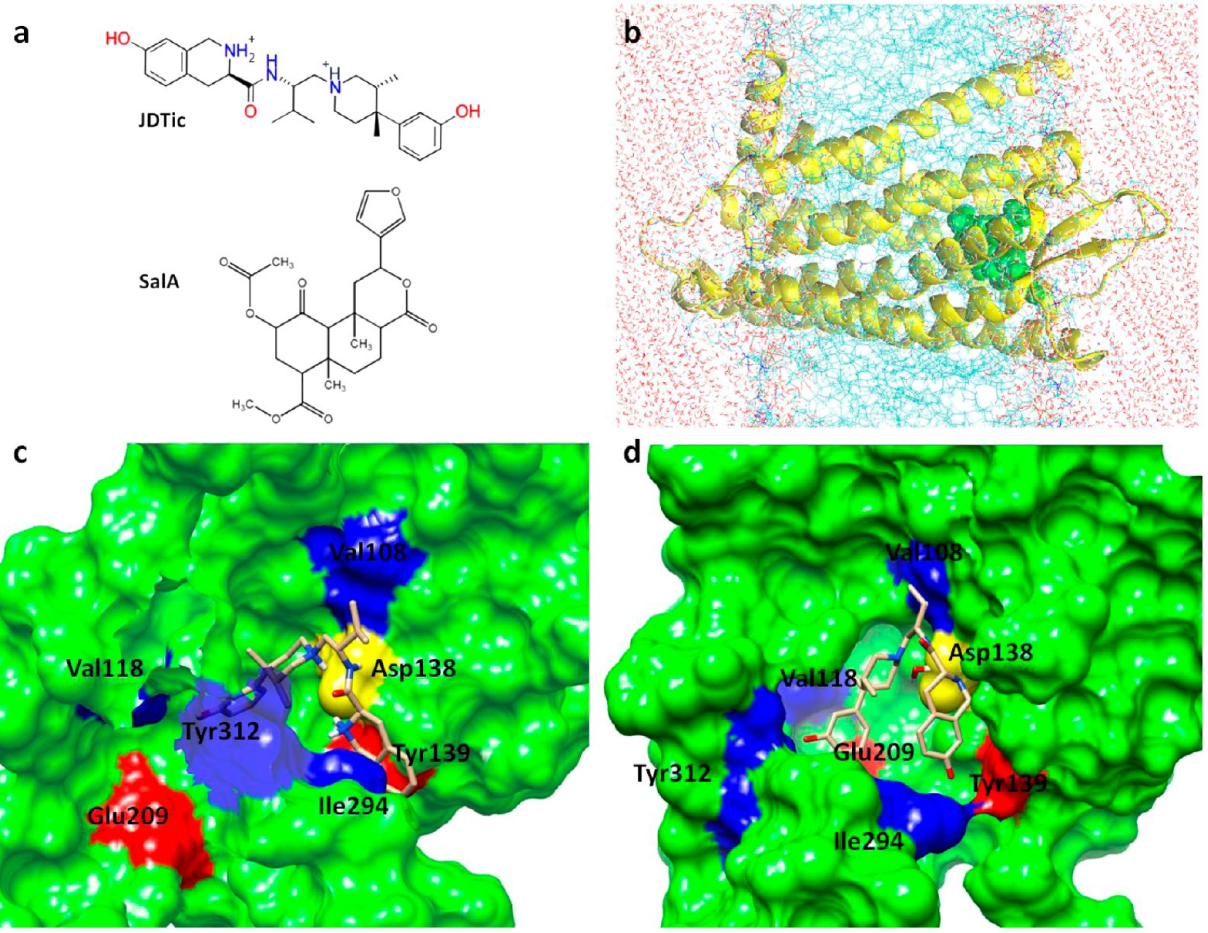

Figure 1. (**a**) Chemical structures of JDTic and SalA. (**b**) Antagonist JDTic (green) bound to human κ-OR (yellow); the complex is merged into a DPPC lipid bilayer (blue) surrounded by water molecules (red). JDTic into the binding site of κ-OR, as depicted by (**c**) the crystal structure,[8] and (**d**) the representative structure after 100 ns of MD simulation. Residues that are implicated in κ-OR selectivity of JDTic are shown in blue, residues participating in hydrogen bond interactions with JDTic (after the MD calculation) are shown in red, and Asp138 is shown in yellow.

divinorum, has been found to be a highly selective κ-OR agonist (Figure 1a).[17,18] Stevens and co-workers have recently reported the crystal structure of human κ-OR in complex with JDTic[19,20] (a κ-OR antagonist in early stages of clinical trials, Figure 1a) at 2.9 Å resolution.[8] Their findings include information on the structure, molecular recognition and selectivity of κ-OR.

The recent availability of high-resolution GPCR structures supports the observation that the receptors are dynamically flexible, and their functions can be modulated by several factors. In this consideration, molecular dynamics (MD) appear to be crucial when studying GPCR versatility associated with functioning and ligand recognition. Indeed, for example Shaw and co-workers performed long MD simulations to reveal the pathway and drug binding mechanism in β_1 and β_2 adrenergic receptors;[21] Heifetz et al. combined homology modeling of orexin receptors with MD to describe the selectivity and binding of several antagonists;[22] Provasi et al. used the prototypic β_2 adrenergic receptor to show that ligands with diverse efficacies induce different GPCR conformations that trigger different biological responses;[23] in two other articles, Provasi et al. proposed the following: (i) activation pathways of the bovine rhodopsin after performing free energy calculations from biased MD[24] and (ii) possible entrance pathways of antagonist naloxone into the binding cavity of δ-OR;[25] Tosh et al. employed *in silico* fragment screening for adenosine receptor agonists, and they identified several promising derivatives;[26] also, molecular docking calculations have been successfully combined with crystallographic data to describe agonist binding to adenosine receptor;[27] finally, QSAR studies have been used to predict the binding affinity of SalA analogs to κ-OR.[28]

Here, we employ a variety of computational approaches to elucidate the mechanism by which JDTic and SalA bind to κ-OR. Our methodology included the following: 1) all-atom, unrestrained MD simulations of JDTic−κ-OR and SalA−κ-OR in explicit water and in lipid bilayers (DPPC), to describe and compare the conformational properties and interactions between the two complexes; 2) Molecular Mechanics Poisson−Boltzmann Surface Area (MM−PBSA) free energy calculations to estimate the binding affinities and to decompose them into contributions from different types of interactions; 3) MD simulation of apo κ-OR to compare the behavior of the complexes to the unbound receptor; 4) Atoms in Molecules (AIM) and Su and Li *ab initio* calculations for rigorous energy estimation. The crystal structure provides information regarding conformations and principal interactions in the κ-OR complex; however, only a static, average description of the system can be offered. Since it has been widely formulated that GPCR structures are rather mobile and alternate between "active" and "inactive" states,[1,29] a thorough approach that describes the evolution of the system is required. Our results reveal the dynamic behavior, structural properties, and the energetic contributions that govern binding. This study is a

dx.doi.org/10.1021/ci5002873 | J. Chem. Inf. Model. XXXX, XXX, XXX−XXX

comprehensive description at the molecular level of two drug-bound κ-OR complexes in aqueous and in lipid bilayer media, thus essentially complementing the crystallographic information.

II. METHODS

II.1. Molecular Dynamics Simulations. The monomer of κ-OR as obtained from the crystal structure was used for the MD simulations. Initial coordinates for the JDTic complex correspond to the following PDB code: 4DJH.[8] The SalA complex was constructed after removing JDTic and docking SalA into the receptor with DOCK 6.[30] Missing residues Thr302−Ser303−His304−Ser305−Thr306 have been included to the structure with Modeller 9.10,[31,32] and side chains have been added with SCWRL4.[33] After a long minimization in implicit solvent (with 10 kcal mol^{-1} $Å^{-2}$ restraints on the receptor atoms) with AMBER 11 software package,[34,35] the structure was evaluated with WHAT_CHECK[36] from WHAT IF Protein Model Check.[37] Crystal water molecules were retained in the structures, and missing hydrogen atoms were added with the tLEaP module of AMBER 11. tLEaP was also used to create the disulfide bond between Cys131 and Cys210. Protonation states and pK_a values for histidine residues were predicted with PROPKA[38,39] under the PDB2PQR (v. 1.8) server.[40] Experimental pK_a predictions suggested a diprotonated state for JDTic at pH 7.[41] Asp138 was considered to be negatively charged and deprotonated to interact with positively charged amino groups of JDTic (Figure 1a). Atomic partial charges, bond lengths, bond and dihedral angles, force constants, and van der Waals parameters for κ-OR were assigned according to the AMBER ff99SB force field.[42] JDTic and SalA preparation was done as follows: missing hydrogen atoms were added with UCSF Chimera.[43] Next, the geometry of the ligands was optimized with Gaussian 09,[44] using the HF/6-31G* basis set. The ANTECHAMBER module was used to derive the RESP atomic partial charges for each drug, and the general AMBER GAFF force field was employed to obtain the force field parameters.[45] The systems were neutralized in tLEaP with the addition of Cl^- counterions (7 and 5 Cl^- for JDTic and SalA complexes, respectively) and were solvated with approximately 28,000 water molecules. Explicit solvation has been represented by the TIP3P water model[46] in truncated octahedral periodic boundary conditions, with a cutoff distance of 10 Å. Long range electrostatic interactions have been calculated using the particle mesh Ewald (PME) method.[47] A four-step, extensive energy minimization process with a steepest descent algorithm (followed by conjugate gradient) was used to diminish steric interactions. First, the solute (ligand−κ-OR complex) was kept almost fixed with a harmonic force constant 500 kcal mol^{-1} $Å^{-2}$, while the water molecules were allowed to relax. The strength of the restraint was gradually reduced in two steps from 10 to 2 kcal mol^{-1} $Å^{-2}$. Finally, the restraint was removed to allow all atoms to move freely. Each of the four steps was performed in 5,000 cycles with a nonbonded cutoff 20 Å. After minimization, each system was heated over 100 ps under constant volume, with the gradual increase of the temperature from 0 to 310 K. The SHAKE algorithm[48] was applied to constrain bond lengths involving hydrogen atoms to their equilibrium distance, thus enabling the use of 2 fs time step. The Langevin thermostat[49] with a collision frequency of 2.0 ps^{-1} was used to keep an average temperature at 310 K. A restraint of 10 kcal mol^{-1} $Å^{-2}$ was applied to the solute; the restraint was retained for the next 100 ps of constant-pressure equilibration. A last equilibration procedure of 100 ps was realized under constant pressure with the entire system unrestrained. Finally, all-atom, unrestrained MD simulations in the NPT ensemble were continued for 100 ns for each receptor complex with the PMEMD program under AMBER 11.[34,35] The Langevin thermostat, SHAKE, and a 10 Å nonbonded cutoff were applied during the heating, equilibration, and production MD periods. Additionally, a 100 ns MD simulation of apo κ-OR has been performed to compare the behavior of the complexes to the unbound GPCR. Subsequent analysis (RMSD, fluctuations, distances, angles, and HB calculations) was performed on the resulting trajectories with the ptraj module of AMBER. Cutoffs of 3.5 Å for the donor−acceptor distance and of 120° for the donor−hydrogen−acceptor angle have been applied to define HB interactions. Also, a 100 ns MD simulation has been carried out for free JDTic in water. Clustering has been realized with MOIL-View 10.0,[50] based on a hierarchical algorithm. A 1.5 Å RMSD cutoff was introduced to assign 10,000 JDTic conformations (bound to κ-OR) into distinct clusters; for clustering the conformations of unbound JDTic in water, a 2.0 Å RMSD cutoff was applied.

Representative conformations (the frame that has the lowest RMSD against the average structure) of JDTic−κ-OR and SalA−κ-OR were used as input structures for simulations in DPPC membranes. Membrane simulations were further continued for another 20 ns with NAMD.[51]

II.2. MM−PBSA Calculations. MM−PBSA is a method that calculates free energy differences between two states.[52−55] Therefore, binding affinities can be estimated; additionally, decomposition into contributions from different types of interactions may be obtained. The partition of the binding free energy into contributions sheds light into the process of complex formation. For each ligand−receptor system, the binding free energy change (ΔG_{bind}) involves the binding process:

$$\text{Receptor} + \text{Ligand} \rightarrow \text{Complex}$$

The procedure was applied on 10,000 snapshots of the trajectories that did not contain water molecules or counterions. Snapshots were equally spaced at 10 ps intervals to ensure uncorrelated structures.[52] For every snapshot, the binding free energy is calculated with the following equation

$$\Delta G_{bind} = G_{complex} - (G_{receptor} + G_{ligand}) \quad (1)$$

where ΔG_{bind} is the total binding free energy, and $G_{complex}$, $G_{receptor}$, and G_{ligand} are the respective energies for the complex, the receptor (κ-OR), and the ligand (JDTic or SalA). The binding energy can be divided in enthalpy and entropy contributions:

$$\Delta G_{bind} = \Delta H - T\Delta S \quad (2)$$

The enthalpy of binding is

$$\Delta H = \Delta E_{MM} + \Delta G_{sol} \quad (3)$$

where ΔE_{MM} is the interaction energy between receptor and ligand (computed with the molecular mechanics method), and ΔG_{sol} is the change in solvation free energy upon ligand binding.

ΔE_{MM} is further divided into

$$\Delta E_{MM} = \Delta E_{elec} + \Delta E_{vdW} \quad (4)$$

ΔE_{elec} is the electrostatic interaction energy, and ΔE_{vdW} is the van der Waals interaction energy. Calculation of these two

dx.doi.org/10.1021/ci5002873 | J. Chem. Inf. Model. XXXX, XXX, XXX−XXX

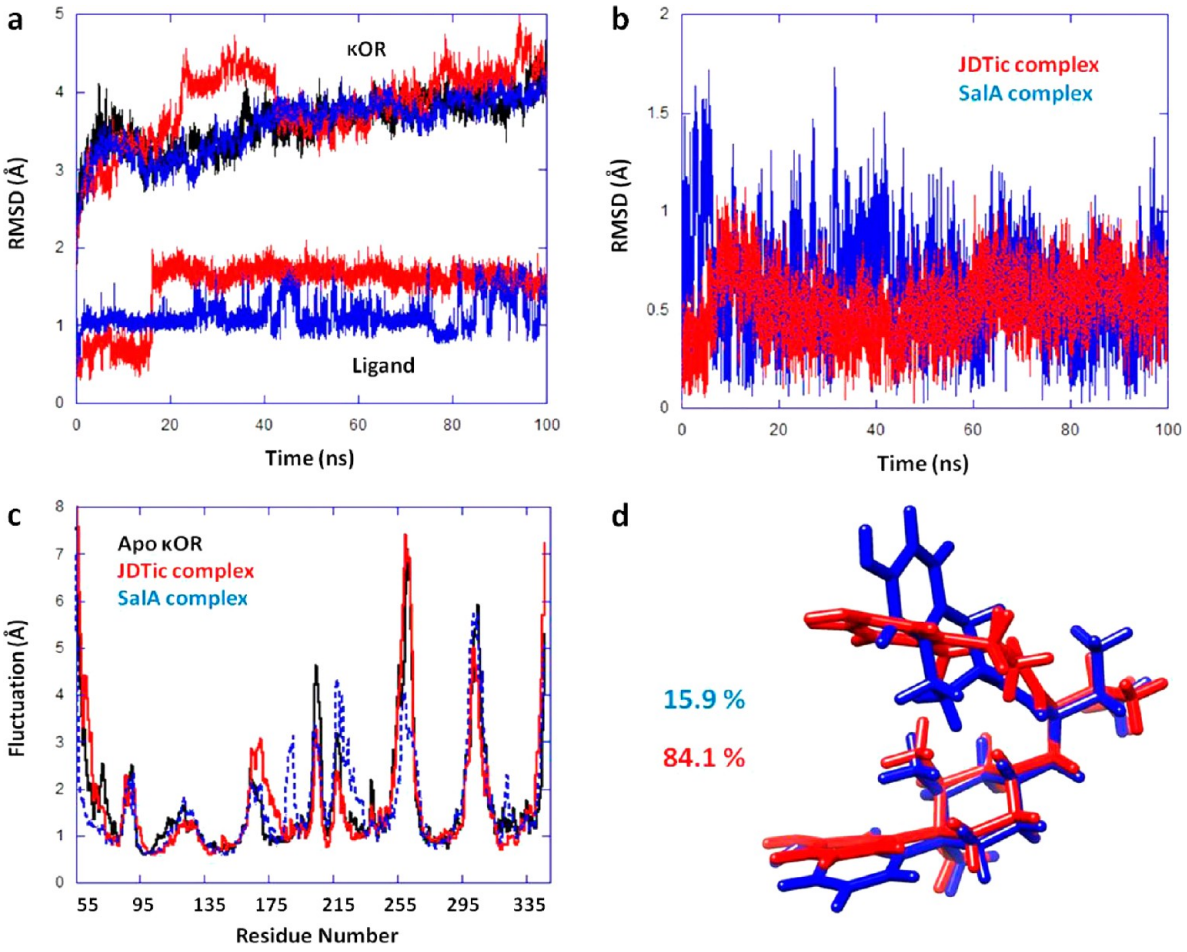

Figure 2. (**a**) **Top:** RMSD for Cα atoms of κ-OR residues in JDTic-bound form (red), SalA-bound form (blue), and unbound (apo) form (black). **Bottom:** RMSD for all atoms of JDTic (red) and SalA (blue) in κ-OR complexes; (**b**) RMSD for Cα atoms of κ-OR residues participating in hydrogen bonds with JDTic (Asp138, Tyr139, Glu209) and with SalA (Gln115, Leu212, His291); (**c**) Cα atomic fluctuations of κ-OR residues in its ligand-bound and apo forms; (**d**) Representative structures of the two dominant JDTic conformations into κ-OR (in water), after clustering analysis. Percentages denote the population of each cluster.

terms has been done without applying any cutoff. The solvation energy (eq 3) combines the electrostatic (ΔG_{PB}) and the nonpolar (ΔG_{NP}) contributions:

$$\Delta G_{sol} = \Delta G_{PB} + \Delta G_{NP} \quad (5)$$

The electrostatic energy (ΔG_{PB}) is approximated by the Poisson−Boltzmann (PB) method,[56] using the PBSA module of AMBER, and the hydrophobic contribution to solvation (ΔG_{NP}) is calculated through estimation of the solvent-accessible surface area (SASA):

$$\Delta G_{NP} = \gamma^{*}\mathrm{SASA} + \beta \quad (6)$$

The surface tension, γ, and the offset, β, have been assigned the standard values of 0.005420 kcal mol^{-1} Å^{-2} and −1.008000 kcal mol^{-1}, respectively. ΔG_{NP} was computed with the linear combinations of pairwise overlaps (LCPO) method.[57] In SASA calculation, a probe radius of 1.4 Å has been used for the solvent. The values for the dielectric constants of water and solute were set to 80.0 and 1.0, respectively.[58] The entropy contribution (eq 2) was estimated with normal-mode analysis as performed by the mmpbsa_py_nabnmode program of AMBER 11, over 200 snapshots for computational efficiency. Since normal mode calculations are computationally very demanding, it is recommended to use a smaller number of frames for the entropy calculation compared to PB calculations.[59] The nab routine calculates normal modes in Generalized Born solvent, and it is advantageous compared to earlier versions regarding minimization convergence pitfalls. The ionic strength was set to 0.1 M.

II.3. Localized Molecular Orbital Energy Decomposition Analysis. According to the method of Su and Li[60] the interaction energy, ΔE, is given by

$$\Delta E = E^{el} + E^{ex} + E^{rep} + E^{pl} + E^{disp} \quad (7)$$

where E^{el} is the electrostatic term involving the Coulomb interaction between monomers, E^{ex} is the exchange contribution, which corresponds to the exchange terms between monomers, and E^{rep} is the repulsion term. The polarization component, E^{pl}, describes the "orbital relaxation energy" moving from the monomer Hartree−Fock (HF) spin orbitals to those of the supermolecule.[60] The dispersion energy, E^{disp}, is the difference between the MP2 and HF interaction energies. Decomposition of ΔE in individual energy terms is advantageous, since it provides direct information on the nature of the interaction. The decomposition analysis was carried out at the MP2 level of theory, using the 6-31G* basis set for all atoms. The basis set superposition error (BSSE) has been corrected with the counterpoise method of Bernardi and Boys.[61] All

dx.doi.org/10.1021/ci5002873 | J. Chem. Inf. Model. XXXX, XXX, XXX−XXX

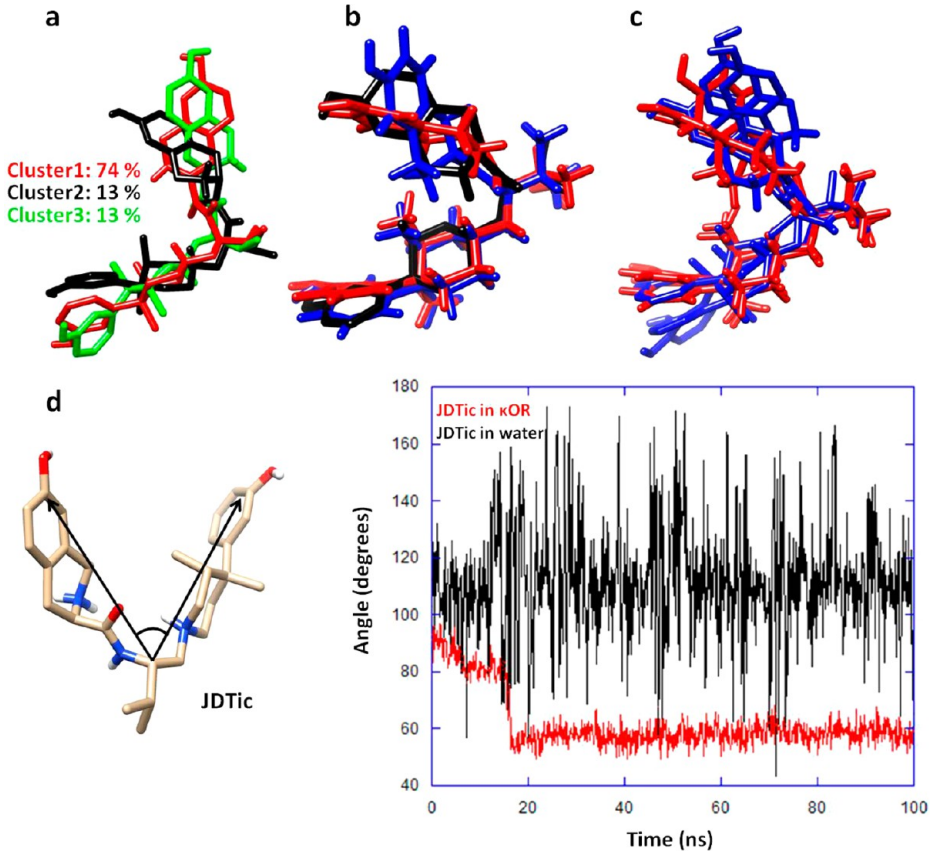

Figure 3. (**a**) Representative structures of the three dominant JDTic conformations in water, after clustering analysis. Percentages denote the population of each cluster; (**b**) Comparison of free JDTic (Cluster 2, black) with the JDTic κ-OR–bound structures from Figure 2d; (**c**) Comparison between the three free (blue) and the two bound (red) JDTic structures; (**d**) Angle variation (left) defines changes in JDTic's shape in water and in κ-OR (right).

computations were performed with the GAMESS quantum chemistry code.[62]

II.4. Atoms in Molecules Approach. The theory of Atoms in Molecules (AIM), as developed by Bader,[63] was used for the study of HB interactions. The main concept of AIM is based on the changes in the electron distribution resulting by either bond or complex formation and allows the study of the nature of the chemical bond and its strength in terms of the electron density distribution function.[63,64] In this context, the topological features of the electron density are analyzed and provide information on the definition of bonding, through the determination of bond paths and bond critical points (BCP). At a BCP, the gradient of the density function, $\nabla\rho(r)$, vanishes. The electron density, $\rho(r)$, and its Laplacian $[\nabla^2\rho(r)]$ can be used to characterize the type of bonding as covalent, ionic, or HB. For H-bonded systems, $\rho(r)$ is $\sim 10^{-2}$, and the Laplacian is positive (0.024–0.139 au).[65]

The energy of the hydrogen bond (E_{HB}) is computed with the following equation[66]

$$E_{HB} \sim \frac{1}{2} V(r)_{BCP} \tag{8}$$

where $V(r)_{BCP}$ is the local potential energy density at the BCP. $V(r)_{BCP}$ is calculated by

$$V(r)_{BCP} = \frac{\hbar^2}{4m}\nabla^2\rho(r)_{BCP} - 2T(r)_{BCP} \tag{9}$$

where $T(r)_{BCP}$ is the local kinetic energy density at the BCP.

The density function $\rho(r)$ was computed with GAUSSIAN at the MP2/6-31+G* level of theory, while all BCPs and Laplacians were computed with the AIM2000 software.[67]

III. RESULTS AND DISCUSSION

In this section, first we investigate the conformational properties of κ-OR upon binding to JDTic and SalA in water and into DPPC lipid bilayer. The MD trajectories were also analyzed to identify hydrogen bond (HB) interactions between the receptor and the ligands. Additionally, the energy of these interactions was estimated by rigorous *ab initio* AIM calculations. Finally, MM–PBSA and *ab initio* (Su and Li) calculations provided an estimation of the binding energies and the main components that drive binding.

III.1. MD Simulations in Water. *III.1.1. Conformational Properties of Inhibitor-Bound and Apo κ-OR Forms.* MD simulations for the JDTic–κ-OR complex (Figure 1b, yellow and green) and the apo form of the receptor in water were initiated from their crystal structures, while SalA was docked into the receptor site as described in Methods. The simulations eventually yielded relatively stable trajectories regarding GPCR backbone structural changes: Cα-based RMSD calculations with respect to the crystal structure showed that κ-OR structures fluctuate slightly around average values, which range between 3.5 and 4 Å (Figure 2a). A noticeable change for the JDTic–κ-OR complex at 18 ns (Figure 2a) may be linked to a structural rearrangement of JDTic inside the receptor. As shown in Figure 1c and 1d, a conformational

dx.doi.org/10.1021/ci5002873 | J. Chem. Inf. Model. XXXX, XXX, XXX–XXX

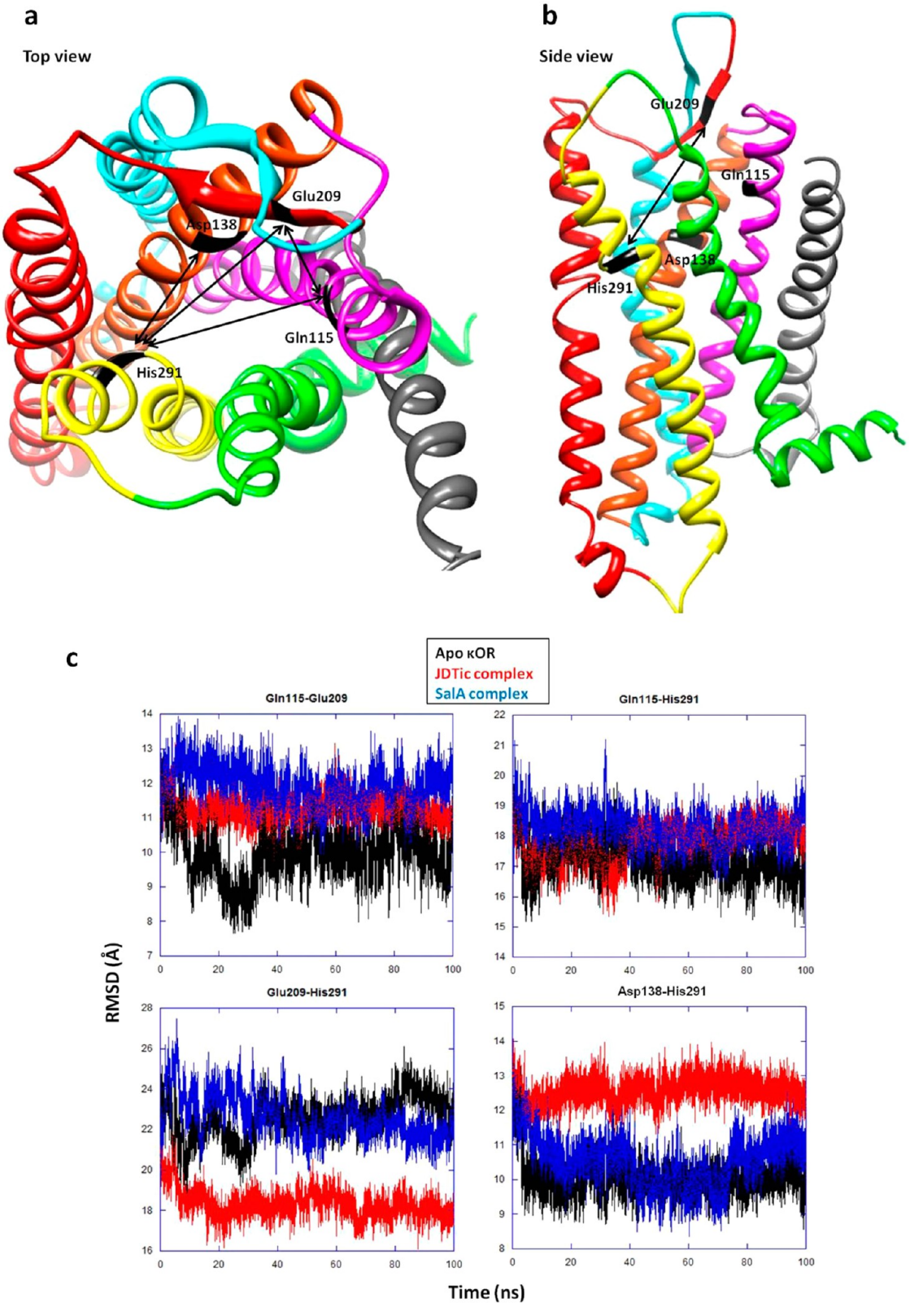

Figure 4. (**a**) Distances between Cα atoms of selected κ-OR residues (black) that define the shape of the binding site. The seven transmembrane domains are in different colors; (**b**) Distance between the binding site−covering loop Glu209 (Cα) and His291 (Cα); (**c**) Distance calculations estimate the size of the binding site in JDTic-bound, SalA-bound, and apo forms of κ-OR.

change of binding site residues induced a proper modification to the shape of the pocket, thus favoring a more closed "V-shape" structure of JDTic. This repositioning of the antagonist may have been due to a rearrangement in HB interactions that stabilize JDTic in the binding site of κ-OR and will be examined in the following paragraphs. After the aforementioned structural change of JDTic, however, the drug remained practically stable throughout the simulation, contrary to SalA, which appeared

dx.doi.org/10.1021/ci5002873 | J. Chem. Inf. Model. XXXX, XXX, XXX−XXX

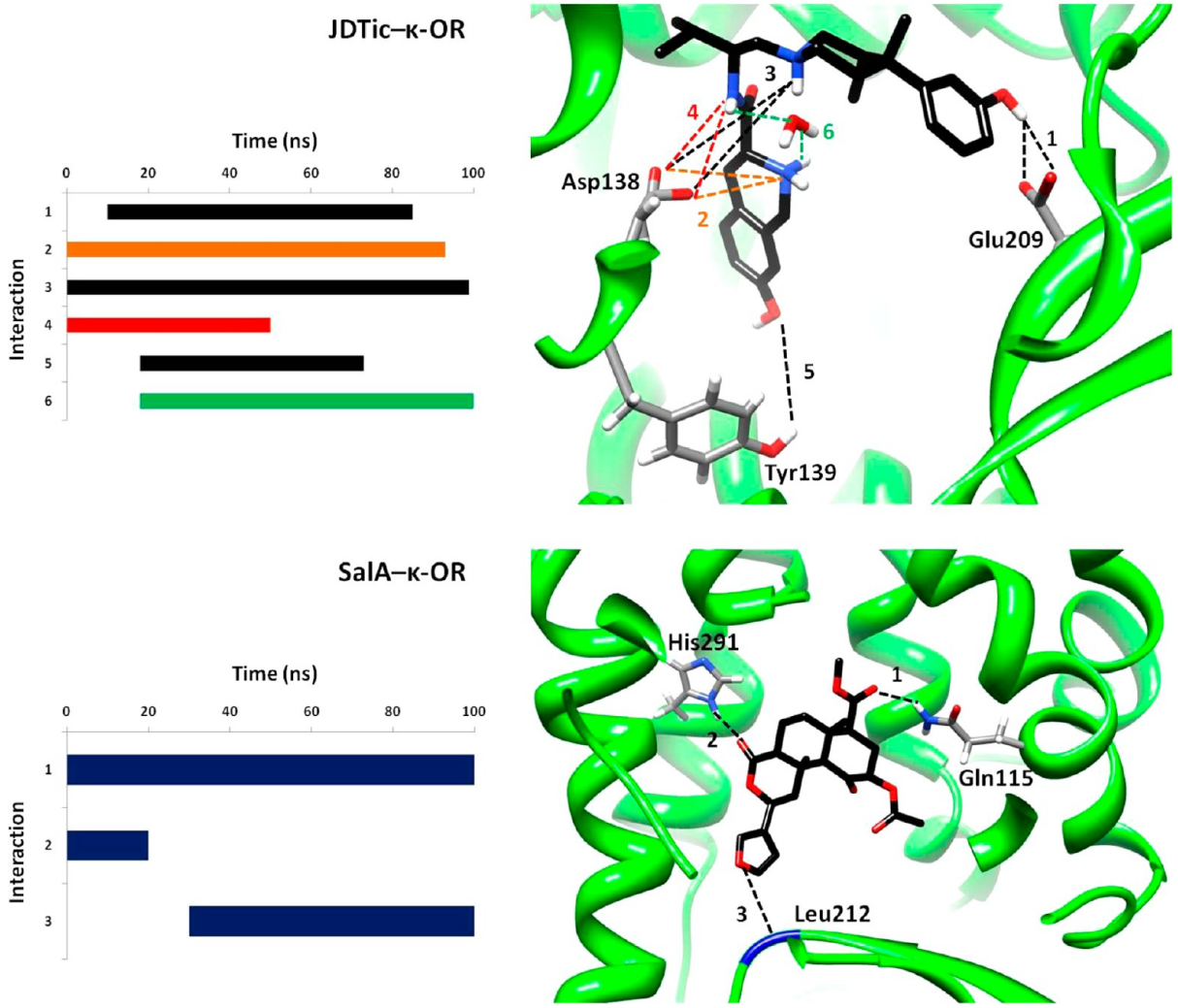

Figure 5. Main hydrogen bond interactions versus time in JDTic–κ-OR and SalA–κ-OR complexes. The numbering on the charts (left) corresponds to the hydrogen bonds shown on the cartoons (right). Chart bars denote the time evolution of HBs and vary in the frequency of HB appearance. A more detailed description of interactions is provided in Tables S2 and S3.

stable for the first ∼40 ns but increased its flexibility during the second half of the simulation (Figure 2a, bottom).

The κ-OR structure in both complexes was stable overall; however, regions of the receptor vary in mobility. Cα atomic fluctuation calculations for each residue revealed that intracellular (e.g., Phe169, Arg257–Leu259) and extracellular regions (e.g., Asp216–Trp221, Gly300–Thr306) appeared highly flexible (Figure 2c). This is anticipated, since they belong to the outer parts of the receptor, being totally exposed to the solvent (Figure S1). Except for these regions, however, most κ-OR residues presented low fluctuations (in both complexes and in apo form); importantly, all residues that were mentioned above to be crucial toward binding showed particularly low fluctuation values.

Clustering calculations for JDTic in κ-OR revealed that the antagonist exists in two (V-shape) major forms. Figure 2d displays the two JDTic representative structures, which differ in the position and orientation of the tetrahydroisoquinoline ring. Superposition of the two structures shows that the rings are perpendicular to each other. Interestingly, clustering calculations on a separate JDTic–water 100 ns trajectory revealed the existence of three forms that differ by at least 2 Å RMSD from each other and showed that ∼13% of the unbound JDTic is in a bent conformation, similar to the one in Figures 1d and 2d (red). The structure comparison is shown in Figure 3a and b. For the remaining 87% of the simulation, it was suggested that free JDTic in water adopts more extended (yet V-shape) forms and is significantly more flexible than when bound to κ-OR (Figure 3c and d). Indeed, the (average ± standard deviation) values for the angle that defines the shape of JDTic (Figure 3d) are 62.14 ± 10.18° and 112.13 ± 19.58° for the drug in κ-OR and in water, respectively. Especially, after the aforementioned structural change at 18 ns, which resulted in a more "closed" conformation for JDTic inside the receptor, the average values for the angle and its variation further diminish (58.05 ± 3.35°, calculations are based on the last 82 ns of the trajectory). The above features of the unbound JDTic may offer enough suppleness to enter the binding pocket and adjust its positioning properly for optimal binding. Indeed, according to Wu et al.,[8] upon insertion of JDTic into κ-OR, the drug adopts a V-shape conformation that is characterized by the proximity of its two amino groups.

To study further the effect of ligand binding on the structure of the receptor, we also investigated the conformational changes of the binding site region in the apo form of κ-OR and when bound to JDTic or SalA. We selected four pairs of

dx.doi.org/10.1021/ci5002873 | J. Chem. Inf. Model. XXXX, XXX, XXX–XXX

Table 1. Energy of Hydrogen Bonds[a] (in kcal/mol) Involving JDTic−κ-OR in Different Charge States of JDTic

	JDTic charge					
hydrogen bond	+2	+1[b]	+1[c]	+1[d]	0[e]	0[f]
O31-H68−Glu209 OE1	−11.98	−12.01	−12.05	−12.05	−12.08	−12.08
N2-H37−Asp138 OD1	−13.05	−13.65		−12.96	−13.55	
N2-H37−Asp138 OD2	−7.72	−7.72		−7.66	−7.66	
N2-H38−H_2O	−7.96		−8.16	−7.94		−8.16
H_2O-Asp138 O[g]	−9.29	−9.47	−9.47	−9.32	−9.51	−9.35
N20-H50−Asp138 OD2	−8.41	−8.35	−8.35			
N14-H45−Asp138 OD2	−10.89	−10.67	−10.67	−10.38	−10.17	−10.13
$E_{HB\ (tot)}$[h]	−69.3	−61.87	−48.70	−60.31	−52.97	−39.72

[a]The MP2/6-31+G* method was used for the computation of the bond critical points. [b]The $H38^+$ proton has been removed (Figure S4). [c]The $H37^+$ proton has been removed (Figure S4). [d]The $H50^+$ proton has been removed (Figure S4). [e]The $H38,50^+$ protons have been removed (Figure S4). [f]The $H37,50^+$ protons have been removed (Figure S4). [g]Figure S3. [h]Sum of the hydrogen bond energies.

binding site residues that have been implicated in κ-OR interactions with ligands[8] (Gln115−Glu209, Gln115−His291, Glu209−His291, Asp138−His291) and considered the distances between Cα atoms of each pair as proper descriptors of the size/shape of the binding site (Figure 4a). It was generally suggested that in the apo form of the receptor the binding site is more confined (Figure 4c, black), while upon ligand binding the transmembrane (TM) domains tend to separate more in order to accommodate the substrate (Figure 4c, red and blue). The average values for each distance are presented in Table S1. Upon binding, JDTic induces greater conformational changes to the binding site than SalA; however, the binding sites of SalA-bound and the apo form of the receptor are more flexible, as shown in Figure 4c. The structural change of the binding site region in the presence of JDTic is defined by a Glu209−His291 approach and an Asp138−His291 separation, compared to the apo or SalA-bound forms (Figure 4c, bottom). It appears that the region containing Glu209 (Asp204−Phe214) forms a loop that covers the binding site, thus entrapping JDTic into the receptor (Figure 4b). The approach of Glu209 and His291 may have facilitated the displacement of the Asp138-containing TM domain (Figure 4a, orange) away from His291 to better accommodate JDTic into the receptor.

III.1.2. Hydrogen Bond Interactions. In this section, we employ the MD results to gain information on the dynamic variation of HBs and perform *ab initio* calculations to estimate the energy associated with these interactions.

Hydrogen bond analysis on the two κ-OR complexes showed that both ligands are stabilized into the receptor via HBs involving residues Asp138, Glu209, Tyr139 (with JDTic), and Gln115, His291, Leu212 (with SalA); the κ-OR binding site with these six HB-participating residues is shown in Figure S2. JDTic-related HB interactions are more frequent and involve multiple ligand/receptor sites, compared to SalA interactions (Figure 5). Contrary to JDTic, SalA lacks any charged groups or nitrogen atoms; it is therefore expected to display diminished interactions. The HBs between the protonated amines of JDTic (Figure 1a) and the side chain of Asp138 totally verified the crystallographic results;[8] moreover, it is noted that the aforementioned structural rearrangement of the binding pocket and the positioning of the drug also facilitated additional HB interactions with Glu209 and Tyr139 (Figure 1d). In accordance with the above, the HB between JDTic and Glu209 may be justified by the Glu209−His291 approach (Figure 4c), which enabled a proper positioning for the drug to interact with Glu209. Also, it was suggested that a water-mediated HB within JDTic altered the shape of the molecule appropriately to favor additional interactions with the binding site of the receptor (Figure 5). Indeed, an intra-JDTic water bridge between the amino groups is formed after ∼18 ns of the simulation, and it coincides with the appearance of the interaction between JDTic and Tyr139 (Figure 5), thus well justifying the structural change of JDTic mentioned above (Figure 2a, bottom). Importantly, the water-mediated interaction within JDTic along with the results of the clustering analysis (Figure 3) are also supported by the aforementioned crystallographic study, where the authors denote the significance of a "bent" JDTic structure for its entrance into the binding pocket.[8] The permanent presence of water molecules in the binding site of opioid receptor structures has been also observed in δ-OR complexes, and the role of water in such systems was discussed by Collu et al.[68] RMSD calculations for κ-OR residues that participate in HBs with either JDTic or SalA are reported in Figure 2b. It was observed that residues involved in interactions with SalA are more flexible than residues forming HBs with JDTic. This denotes the capacity of JDTic to stabilize the structure of the κ-OR binding site more efficiently compared to SalA.

Ab Initio Hydrogen Bond Analysis for JDTic and SalA Complexes. We have considered an average MD structure involving only JDTic and the main residues that participate in HBs (Asp138, Glu209, and Tyr139) for further Atoms in Molecules[63] (AIM) *ab initio* calculations, in order to compute the energy of the HBs associated with the drug and these residues. According to the AIM analysis, all HBs contribute significantly to binding, with energies that range from −8.4 to −13.05 kcal/mol. More specifically, Glu209 forms an HB (bond 1, Figure 5) of −11.98 kcal/mol. The water molecule forms an HB bridge between the NH_2^+ group of the drug (bond 6, Figure 5), with an energy of −7.96 kcal/mol, and a second one with the backbone carbonyl O of Asp138, with an energy of −9.29 kcal/mol (Figure S3). Note that this interaction was not observed during the MD calculations; however, the orientation of JDTic toward Asp138 and their proximity indicate that such an HB is possible. Thus, the role of water is further emphasized, as it may facilitate both intra-JDTic and JDTic−receptor interactions. The carboxyl group of Asp138 forms four HBs with JDTic. Two with NH_2^+ (bond 2, Figure 5) with energies −13.05 and −7.72 kcal/mol, one with the H45 bonded to N14 (bond 3, Figure 5), with energy of −10.89 kcal/mol, and the last one with the H50 bonded to N20 (bond 4, Figure5), with energy of −8.41 kcal/mol. Atom numbering for JDTic is shown in Figure S4.

dx.doi.org/10.1021/ci5002873 | J. Chem. Inf. Model. XXXX, XXX, XXX−XXX

Similarly, another average MD structure including Gln115/Leu212/His291 and SalA (Figure 5) was also considered for AIM calculations. Only the HB between Gln115 and SalA with the energy of −3.07 kcal/mol was predicted.

Hydrogen Bond Energy Dependence on JDTic Charge. We have also considered the JDTic− Asp138/Glu209/Tyr139 truncated system in the different protonation states of JDTic and calculated the HB strength versus charge variation. The results are shown in Table 1 and indicate that JDTic in the diprotonated (+2) form displays stronger interactions with the binding site compared to the other possible charge states. This may be attributed to the larger number of HBs formed between JDTic and Asp138. To facilitate our discussion, we denote the number of HBs with n. For charge state +2, n is equal to 4 (involving JDTic atoms: N2-H37, N20-H50, N14-H45, Figure S4) with a total contribution of −40.07 kcal/mol. Removal of proton $H37^+$ (charge state +1, Figure S4) n decreases to 2, thus contributing −19.02 kcal/mol to the total energy (−48.7 kcal/mol). When removing $H37^+$ and $H50^+$ (charge state 0, Figure S4), n equals 1, contributing only −10.13 kcal/mol. The analysis suggests that alterations in the JDTic charge state (Table 1) change the number of HBs between JDTic and Asp138, thus resulting in a significant effect upon the total HB energy. Finally, we note that the energies of HBs formed between H_2O−JDTic and between Glu209−JDTic remain practically unaffected with the change of the JDTic charge state (Table 1). This is also true for the contribution of the HB between H_2O and the carboxylate of Asp138.

Ab Initio Hydrogen Bond Analysis of Gln115−JDTic and His291−JDTic. We have selected two additional truncated systems, which include the interactions between JDTic and residues Gln115/His291 (Figure S5). MD calculations showed that these amino acids did not participate in direct HBs with the drug; however, they are considered to be important toward binding, since they are in close proximity to the ligand. The employed geometries depict each residue near JDTic and correspond to the average structures derived from the MD simulation (Figure S5).

For the Gln115−JDTic system, the AIM analysis revealed an interaction, with energy −4.95 kcal/mol, while for the His291−JDTic system, the observed interaction has energy of −2.91 kcal/mol. Comparing the distances between JDTic and each residue (Figure S5), it is expected that the larger distance is associated with a weaker interaction and a decrease in $\nabla^2\rho(r)$ and $\rho(r)$. For the C−H---O interaction (Figure S5a), these properties were computed to be 0.014 au and 0.019 au, respectively, while for C−H---N (Figure S5b), they correspond to 0.0107 au and 0.014 au, respectively.

III.1.3. Energetic Analysis. MM−PBSA (Molecular Mechanics Poisson−Boltzmann Surface Area) calculations for the estimation of the binding free energy of the two complexes verified the above structural and interaction analyses. The results of Table 2 demonstrate that JDTic has significantly more effective receptor binding ($\Delta G_{MM-PBSA}$ = −31.6 kcal/mol) than SalA ($\Delta G_{MM-PBSA}$ = −9.8 kcal/mol); however, it was observed that SalA presents adequate binding to κ-OR. We remark that the free energy calculation on the JDTic−κ-OR complex overestimates the experimental measurement (by ≈17 kcal/mol); MM−PBSA is a fast but not very accurate method to calculate absolute binding energies, since it computes the molecular mechanical energies in the presence of a continuum (implicit) solvent model. However, it shows the qualitative direction of ΔG upon complex formation and is widely accepted as a useful tool giving correct ranking of binding energies (and their components) for different inhibitors.[58] Energy decomposition to individual contributions revealed that van der Waals and the electrostatic component of the molecular mechanical energy (ΔE_{elec}) act most favorably toward binding for both complexes. Especially, the electrostatic contribution within the JDTic−κ-OR complex is significantly more pronounced (due to the +2 charge on JDTic) than within SalA−κ-OR. This is in agreement with the crystallographic data, since JDTic has been found to form salt bridge interactions with the side chain of Asp138.[8] However, the role of electrostatic interactions in the formation of κ-OR complexes should be examined by also considering the electrostatic contribution to solvation (ΔG_{PB}) together with ΔE_{elec}. The total electrostatic contribution, $\Delta G_{elec(tot)}$, is positive in both complexes (5.3 and 25.1 kcal/mol, in JDTic and SalA complexes, respectively), since the unfavorable desolvation penalty[69] is not fully compensated by the favorable electrostatics within each complex (Table 2). This suggests that electrostatics disfavor binding of either JDTic or SalA to the receptor. The favorable complex formation, in both cases, is driven by the van der Waals contribution ($\Delta E_{vdW,JDTic}$ = −56.8 kcal/mol, $\Delta E_{vdW,SalA}$ = −52.2 kcal/mol) and the nonpolar contribution to solvation ($\Delta G_{NP,JDTic}$ = −5.0 kcal/mol, $\Delta G_{NP,SalA}$ = −4.1 kcal/mol). This finding is in agreement with several other studies involving interactions among proteins, RNA, and ligands.[70−74] Nevertheless, the main reason for the total binding energy difference between the two complexes is due to the much more unfavorable electrostatics in SalA−κ-OR than in JDTic−κ-OR.

Table 2. Energetic Analysis for κ-OR Complexes with Compounds JDTic and SalA, as Obtained by MM−PBSA Calculations

energy (kcal mol^{-1})	JDTic	SalA
ΔE_{vdW}	−56.80 ± 0.04[a]	−52.17 ± 0.04
ΔE_{elec}	−230.45 ± 0.19	−12.62 ± 0.07
$\Delta E_{MM,\ gas}$	−287.25 ± 0.19	−64.79 ± 0.05
ΔG_{PB}	235.78 ± 0.14	37.74 ± 0.05
$\Delta G_{elec(tot)}$[b]	5.34 ± 0.08	25.12 ± 0.06
ΔG_{NP}	−4.97 ± 0.00	−4.05 ± 0.00
ΔG_{solv}	230.82 ± 0.14	33.69 ± 0.05
$\boldsymbol{\Delta H_{(MM+solv)}}$	−56.43 ± 0.08	−31.10 ± 0.04
$\boldsymbol{-T\Delta S_{tot}}$	24.87 ± 0.56	21.27 ± 0.53
$\boldsymbol{\Delta G_{MM-PBSA}}$	−31.56 ± 0.11[c]	−9.83 ± 0.08[c]
$\boldsymbol{\Delta G_{exp}}$	−14.35[20,75]	−11.00 to −10.61[76−79]

[a]Errors represent standard errors of the mean (SEM): SEM = standard deviation/$\sqrt{N}$, where N is the number of trajectory frames used in MM−PBSA calculations (200 for entropy and 10,000 for everything else). [b]$\Delta G_{elec(tot)} = \Delta E_{elec} + \Delta G_{PB}$. [c]The error bars for $\Delta G_{MM-PBSA}$ have been estimated as pooled standard errors of the mean based on the formula $S = (((n_1 - 1)(s_1)^2 + (n_2 - 1)(s_2)^2)/(n_1 + n_2 - 2))^{1/2}$, where n_1 is the number of frames for the ΔH calculation (n_1 = 10,000), n_2 is the number of frames for the $-T\Delta S$ calculation (n_2 = 200), and s_1 and s_2 are the standard errors of the mean of ΔH and $-T\Delta S$ calculations, respectively.

Per-Residue Free Energy Decomposition. Energy decomposition in a per-residue basis may also provide useful information on individual contributions to binding. For JDTic−κ-OR and SalA−κ-OR complexes, the interaction of each residue with the rest of the system is presented in Figure 6. As expected, JDTic−κ-OR residues have more favorable contributions to the binding energy than SalA−κ-OR residues.

dx.doi.org/10.1021/ci5002873 | J. Chem. Inf. Model. XXXX, XXX, XXX−XXX

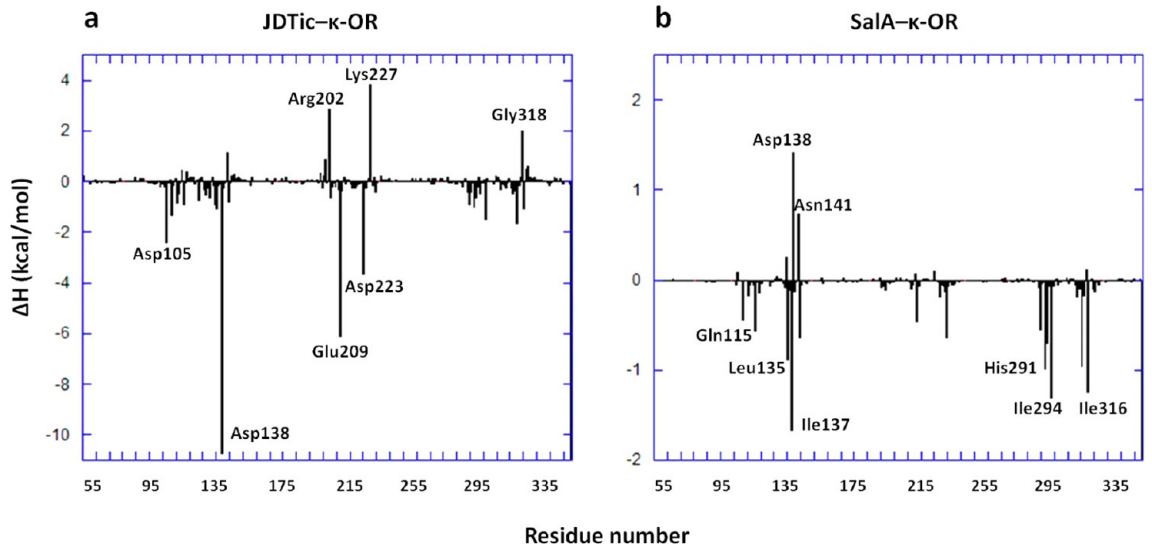

Figure 6. Per residue MM–PBSA decomposition analysis in (**a**) JDTic–κ-OR and (**b**) SalA–κ-OR complexes. Note the difference in the *y*-axis scale between the two complexes.

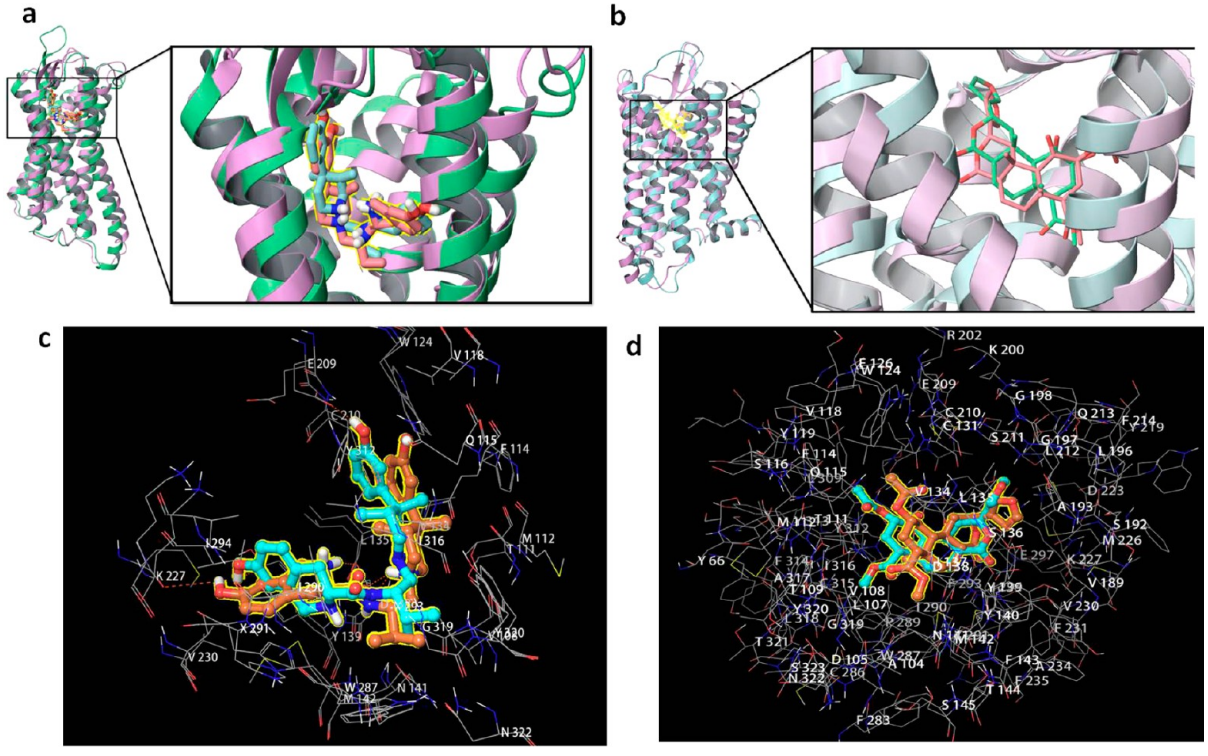

Figure 7. (**a**) Superimposition of representative structures of receptor–JDTic in water (shown in green ribbons) with receptor–JDTic in lipid bilayer (shown in purple ribbons). RMSD = 2.9 Å; (**b**) Superimposition of representative structures of receptor–SalA in water (shown in green ribbons) with receptor–SalA in lipid bilayer (shown in purple ribbons). RMSD = 3.2 Å; Superimpositions of ligands (**c**, JDTic), (**d**, SalA), and active sites of representative structures.

In particular, residues Asp138 and Glu209 that participate in HB interactions with JDTic have the greatest contribution toward complex formation; Asp105/223 also appear crucial for efficient JDTic binding (Figure 6a). In the SalA–κ-OR complex, the most favorable binding energy contributions were attributed to Ile137/294/316, Leu135, and His291/Gln115 (also HB-participating residues with SalA). Interestingly, Asp138 acts against SalA binding to κ-OR (Figure 6b). Further energy decomposition into side chain and backbone contributions revealed that in both complexes ligand binding is driven mostly by interactions involving the side chains of the residues (Figure S6). Finally, the individual JDTic and SalA contributions with κ-OR were calculated to be −22.5 and −14.7 kcal/mol, respectively. A more detailed description of per residue contributions, also for other important (active site, extra- or intracellular loops, etc.) residues in both complexes (including electrostatic and van der Waals components) is provided in Tables S4 and S5. It was observed that extra- or intracellular loops do not contribute significantly, while residues

dx.doi.org/10.1021/ci5002873 | J. Chem. Inf. Model. XXXX, XXX, XXX–XXX

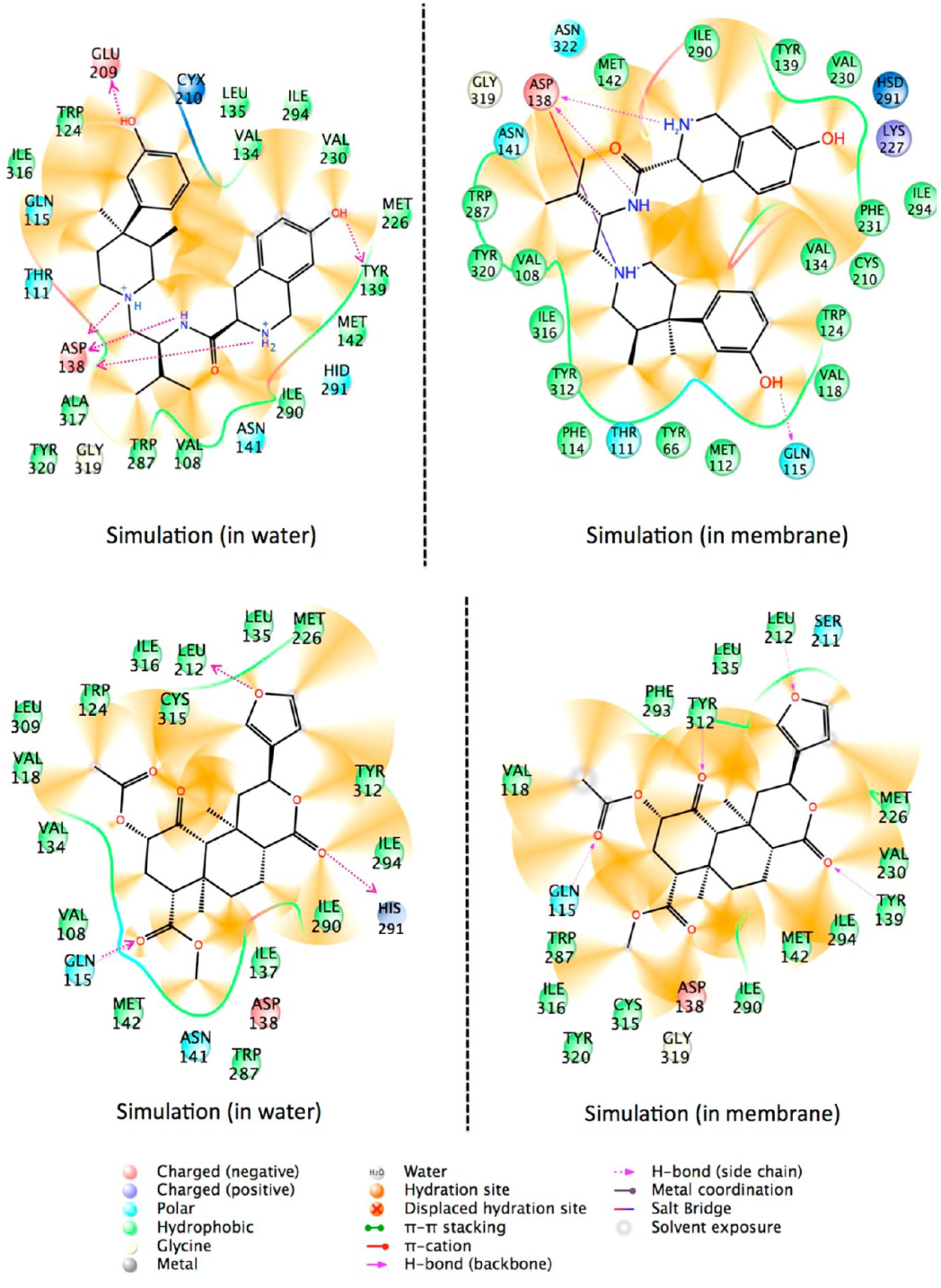

Figure 8. Ligand interaction diagrams of κ-OR–JDTic (top) and of κ-OR–SalA (bottom) in water (left) and in membrane (right).

considered to be important toward ligand selectivity for κ-OR favor JDTic/SalA binding.

Interaction Energy Estimation. Application of the more rigorous *ab initio* Su and Li methodology[60] to the fragment of JDTic–κ-OR (JDTic–Asp138/Tyr139/Glu209) agreed with the MM–PBSA findings and revealed that the larger number of HBs and the positive charge on JDTic are associated with a considerably larger interaction energy (ΔE), when compared to SalA–κ-OR fragment (SalA–Gln115/Leu212/His291). Indeed, it was shown that in JDTic the terms which favor binding ($E^{el} + E^{ex} + E^{pl} + E^{disp}$) account for −533.30 kcal/mol energy gain, while for SalA the corresponding value is only −18.05 kcal/mol. This major difference can be attributed to the fact that the positively charged JDTic and the negatively charged residues (Glu209 and Asp138) result in a stronger electrostatic interaction, which dominates binding. In particular, our analysis showed that the electrostatic contribution in JDTic–κ-OR is −307.3 kcal/mol, namely 58% of ΔE. Contrary to JDTic, the electrostatic contribution for SalA accounts for −6.9 kcal/mol or 38% of the total. Importantly, this is in a qualitative agreement with the MM–PBSA results (ΔE_{elec}, Table 2), thus validating our computational approach.

Energetic Analysis of Gln115–JDTic and His291–JDTic with the ab Initio Su and Li Method. Interaction energy

dx.doi.org/10.1021/ci5002873 | J. Chem. Inf. Model. XXXX, XXX, XXX–XXX

calculations on the JDTic−κ-OR fragments mentioned in the hydrogen bond section (Gln115−JDTic and His291−JDTic) showed that in Gln115−JDTic, ΔE = −4.89 kcal/mol, while in His291−JDTic ΔE = −2.13 kcal/mol. This difference may be attributed to the sum of the negative terms (E^{el} + E^{ex} + E^{pl} + E^{disp}), which is slightly larger in Gln115−JDTic (−36.25 kcal/mol) than in His291−JDTic (−35.7 kcal/mol).

III.2. MD Simulations in DPPC Lipid Bilayer. GPCRs express their functionality in a membrane environment. Therefore, in order to investigate the membrane effect to conformational dynamics of ligands and target, the above systems have been merged into a lipid bilayer (Figures 1b and S7) using the CHARMM-GUI Membrane Builder[80,81] with the OPM module.[82] Systems' stability throughout the simulations has been verified with all-atom (Figure S8a), Cα atoms (Figure S8b), HB residues (Figure S8c), and ligands (Figure S8d) RMSD calculations. While transmembrane (TM) regions were very stable during the simulation (with fluctuations ranging between 0.5 and 1 Å), intracellular and extracellular loops appeared very flexible (up to 3.5 Å, Figure S8e). The RMSD of each frame was screened against the average structure, and the frame with the lowest RMSD was selected as representative structure for the complex (Figure S8f).

Superimposition of representative structures for the two sets of simulations (in water and in lipid bilayer systems) showed similar conformations for the ligands when bound to κ-OR, either in water or into the bilayer (Figure 7). However, a difference was observed between JDTic conformations, where the representative structure in the membrane resembles the least populated cluster in water (Figure 2d, blue). Comparison of ligand−receptor interactions between water and lipid environments revealed that the main HBs (observed in water) are conserved upon system insertion into the lipid bilayer. The reorientation of the tetrahydroisoquinoline ring of JDTic, as expected resulted in abolishment of the HB with Tyr139 (Figure 8). On the other hand, two additional HBs were observed between SalA and κ-OR: interactions with Tyr139 and Tyr312 stabilize further SalA into the binding pocket of the receptor (Figure 8).

Apart from the amino acids that are involved in HBs with the ligands, the publication by Stevens and co-workers identified κ-OR residues Val108, Val118, Trp287, Ile294, and Tyr312 as particularly important in ligand's selectivity for the receptor, since it was shown that they interact with JDTic uniquely in κ-OR, among other closely related ORs.[8] Our HB analysis did not show any major HBs between these residues and JDTic; however, significant hydrophobic interactions were observed (Figure 8). Interestingly, the above residues interact hydrophobically also with SalA. RMSD values for the five residues suggested that JDTic-bound and apo forms of the receptor undergo similar structural changes, whereas SalA-bound form deviates from this pattern (Figure S9). Such a behavior is anticipated, since agonist−κ-OR complexes are expected to show greater changes than antagonist−κ-OR complexes.

IV. CONCLUSIONS

Dynamics, interactions, and binding properties of the human κ-opioid receptor (κ-OR) in complexes with antagonist JDTic and agonist Salvinorin A (SalA) have been calculated by means of molecular dynamics and *ab initio* (AIM and Su and Li) approaches. The availability of the JDTic−κ-OR crystal structure enabled us to elucidate the opioid drug binding mechanism and action. The valuable, yet average description offered by the crystal structure conceals important features of such a dynamic system. Here, we explored the dynamic behavior of κ-OR complexes to identify for the first time the properties that govern ligand binding to the receptor. Our analysis led to the following elements regarding the binding mechanism in κ-OR:

(1) Bound receptor structures (in water and lipid bilayer environments) were significantly stable, except particular extracellular and intracellular regions that appeared expectedly flexible.

(2) In agreement with the crystal data, HB analysis showed that JDTic is stabilized inside the binding site through multiple HBs that involve mostly Asp138. After 18 ns of the simulation, the binding site of the receptor was eventually rearranged to allow the repositioning of the ligand. This structural change involved the approach of loops containing Glu209 and His291 and the simultaneous separation of loops containing Asp138 and His291. This resulted in the formation of additional HBs between JDTic and Glu209. Glu209 appears to be crucial toward binding, since it belongs to an extracellular loop that controls the entrance and entrapment of ligands into the binding site of the receptor. SalA also displayed HBs with binding site residues Gln115, His291, and Leu212, but it has more flexibility than JDTic.

(3) A water molecule mediated an intra-JDTic interaction that induced a "V-shape" to the ligand, with the subsequent formation of an additional HB with Tyr139. The role of water was further emphasized, as it was shown that also forms an HB bridge between JDTic and Asp138.

(4) JDTic in κ-OR exists in two major "V-shape" forms, which differ in the orientation of the tetrahydroisoquinoline ring, while the drug in water alternates between similar structures and more extended conformations. This feature may offer enough flexibility to the drug in order to enter the binding site and adjust properly for optimal binding.

(5) MD calculations in membrane complexes showed similar behavior with the systems in water. Moreover, SalA was further stabilized via hydrogen bonds with Tyr139/312, while the Tyr139 interaction was not observed in the representative structure of the JDTic complex.

(6) Binding free energy calculations showed that both ligands induce favorable complex formation (ΔG_{JDTic} = −31.6 kcal mol^{-1}, ΔG_{SalA} = −9.8 kcal mol^{-1}), mainly driven by van der Waals interactions and the nonpolar contribution to solvation. However, JDTic displayed significantly more efficient binding compared to SalA due to differences in electrostatic interactions. It was also revealed that the most favorable contributions to binding involve side chain interactions of residues Asp138, Glu209, Asp105, Asp223 (JDTic), and Ile137/294/316, Leu135, His291, Gln115 (SalA). The free energy calculations were qualitatively validated by the experimental values ($\Delta G_{JDTic,exp}$ = −14.4 kcal mol^{-1}, $\Delta G_{SalA,exp}$ = −10.8 kcal mol^{-1}).

■ ASSOCIATED CONTENT

Supporting Information

Figures showing the structure of important κ-OR regions, water-mediated hydrogen bonds, RMSD of selected residues, structural analysis of complexes into the lipid bilayer, AIM and per-residue energy decomposition analyses. Tables showing distances that define the shape of κ-OR binding site, hydrogen bonds, per-residue energy decomposition analysis. This ma-

dx.doi.org/10.1021/ci5002873 | J. Chem. Inf. Model. XXXX, XXX, XXX−XXX

terial is available free of charge via the Internet at http://pubs.acs.org.

AUTHOR INFORMATION

Corresponding Authors

*G.L.: e-mail, gleonis@eie.gr.
*M.G.P.: e-mail, mpapad@eie.gr.

Notes

The authors declare no competing financial interest.

ACKNOWLEDGMENTS

G.L. thanks Drs. Seva Katritch, Phil Mosier, and Ray Stevens for discussions. The research leading to these results has received funding from the European Union Seventh Framework Programme (FP7/2007-2013) under grant agreement no. 309837 (NanoPUZZLES project).This work was also supported by the European Commission for the FP7-REGPOT-2009-1 Project 'ARCADE' (Grant Agreement No. 245866). S.D. acknowledges support from Bilim Akademisi - The Science Academy, Turkey under the BAGEP program, and S.D. and R.E.S. acknowledge TUBITAK ULAKBIM High Performance and Grid Computing Center (TR-Grid) as well as National Center for High Performance Computing (Ulusal Yüksek Başarımlı Hesaplama Merkezi- UHeM) for support of computational sources.

REFERENCES

(1) Kolb, P.; Klebe, G. The golden age of GPCR structural biology: any impact on drug design? *Angew. Chem., Int. Ed. Engl.* **2011**, *50*, 11573−11575.

(2) Stevens, R. C.; Cherezov, V.; Katritch, V.; Abagyan, R.; Kuhn, P.; Rosen, H.; Wuthrich, K. The GPCR Network: a large-scale collaboration to determine human GPCR structure and function. *Nat. Rev. Drug Discovery* **2013**, *12*, 25−34.

(3) Hausch, F.; Holsboer, F. The seven pillars of molecular pharmacology: GPCR research honored with Nobel Prize for chemistry. *Angew. Chem., Int. Ed. Engl.* **2012**, *51*, 12172−12175.

(4) Cherezov, V.; Rosenbaum, D. M.; Hanson, M. A.; Rasmussen, S. G.; Thian, F. S.; Kobilka, T. S.; Choi, H. J.; Kuhn, P.; Weis, W. I.; Kobilka, B. K.; Stevens, R. C. High-resolution crystal structure of an engineered human beta2-adrenergic G protein-coupled receptor. *Science* **2007**, *318*, 1258−1265.

(5) Chien, E. Y.; Liu, W.; Zhao, Q.; Katritch, V.; Han, G. W.; Hanson, M. A.; Shi, L.; Newman, A. H.; Javitch, J. A.; Cherezov, V.; Stevens, R. C. Structure of the human dopamine D3 receptor in complex with a D2/D3 selective antagonist. *Science* **2010**, *330*, 1091−1095.

(6) Jaakola, V. P.; Griffith, M. T.; Hanson, M. A.; Cherezov, V.; Chien, E. Y.; Lane, J. R.; Ijzerman, A. P.; Stevens, R. C. The 2.6 angstrom crystal structure of a human A2A adenosine receptor bound to an antagonist. *Science* **2008**, *322*, 1211−1217.

(7) Shimamura, T.; Shiroishi, M.; Weyand, S.; Tsujimoto, H.; Winter, G.; Katritch, V.; Abagyan, R.; Cherezov, V.; Liu, W.; Han, G. W.; Kobayashi, T.; Stevens, R. C.; Iwata, S. Structure of the human histamine H1 receptor complex with doxepin. *Nature* **2011**, *475*, 65−70.

(8) Wu, H.; Wacker, D.; Mileni, M.; Katritch, V.; Han, G. W.; Vardy, E.; Liu, W.; Thompson, A. A.; Huang, X. P.; Carroll, F. I.; Mascarella, S. W.; Westkaemper, R. B.; Mosier, P. D.; Roth, B. L.; Cherezov, V.; Stevens, R. C. Structure of the human kappa-opioid receptor in complex with JDTic. *Nature* **2012**, *485*, 327−332.

(9) Manglik, A.; Kruse, A. C.; Kobilka, T. S.; Thian, F. S.; Mathiesen, J. M.; Sunahara, R. K.; Pardo, L.; Weis, W. I.; Kobilka, B. K.; Granier, S. Crystal structure of the micro-opioid receptor bound to a morphinan antagonist. *Nature* **2012**, *485*, 321−326.

(10) Hollenstein, K.; Kean, J.; Bortolato, A.; Cheng, R. K.; Dore, A. S.; Jazayeri, A.; Cooke, R. M.; Weir, M.; Marshall, F. H. Structure of class B GPCR corticotropin-releasing factor receptor 1. *Nature* **2013**, *499*, 438−443.

(11) Haga, K.; Kruse, A. C.; Asada, H.; Yurugi-Kobayashi, T.; Shiroishi, M.; Zhang, C.; Weis, W. I.; Okada, T.; Kobilka, B. K.; Haga, T.; Kobayashi, T. Structure of the human M2 muscarinic acetylcholine receptor bound to an antagonist. *Nature* **2012**, *482*, 547−551.

(12) Kruse, A. C.; Hu, J.; Pan, A. C.; Arlow, D. H.; Rosenbaum, D. M.; Rosemond, E.; Green, H. F.; Liu, T.; Chae, P. S.; Dror, R. O.; Shaw, D. E.; Weis, W. I.; Wess, J.; Kobilka, B. K. Structure and dynamics of the M3 muscarinic acetylcholine receptor. *Nature* **2012**, *482*, 552−556.

(13) Hanson, M. A.; Roth, C. B.; Jo, E.; Griffith, M. T.; Scott, F. L.; Reinhart, G.; Desale, H.; Clemons, B.; Cahalan, S. M.; Schuerer, S. C.; Sanna, M. G.; Han, G. W.; Kuhn, P.; Rosen, H.; Stevens, R. C. Crystal structure of a lipid G protein-coupled receptor. *Science* **2012**, *335*, 851−855.

(14) Fredriksson, R.; Lagerstrom, M. C.; Lundin, L. G.; Schioth, H. B. The G-protein-coupled receptors in the human genome form five main families. Phylogenetic analysis, paralogon groups, and fingerprints. *Mol. Pharmacol.* **2003**, *63*, 1256−1272.

(15) Waldhoer, M.; Bartlett, S. E.; Whistler, J. L. Opioid receptors. *Annu. Rev. Biochem.* **2004**, *73*, 953−990.

(16) Carlezon, W. A., Jr.; Beguin, C.; Knoll, A. T.; Cohen, B. M. Kappa-opioid ligands in the study and treatment of mood disorders. *Pharmacol. Ther.* **2009**, *123*, 334−343.

(17) Roth, B. L.; Baner, K.; Westkaemper, R.; Siebert, D.; Rice, K. C.; Steinberg, S.; Ernsberger, P.; Rothman, R. B. Salvinorin A: a potent naturally occurring nonnitrogenous kappa opioid selective agonist. *Proc. Natl. Acad. Sci. U. S. A.* **2002**, *99*, 11934−11939.

(18) Yan, F.; Bikbulatov, R. V.; Mocanu, V.; Dicheva, N.; Parker, C. E.; Wetsel, W. C.; Mosier, P. D.; Westkaemper, R. B.; Allen, J. A.; Zjawiony, J. K.; Roth, B. L. Structure-based design, synthesis, and biochemical and pharmacological characterization of novel salvinorin A analogues as active state probes of the kappa-opioid receptor. *Biochemistry* **2009**, *48*, 6898−6908.

(19) Carroll, I.; Thomas, J. B.; Dykstra, L. A.; Granger, A. L.; Allen, R. M.; Howard, J. L.; Pollard, G. T.; Aceto, M. D.; Harris, L. S. Pharmacological properties of JDTic: a novel kappa-opioid receptor antagonist. *Eur. J. Pharmacol.* **2004**, *501*, 111−119.

(20) Thomas, J. B.; Atkinson, R. N.; Rothman, R. B.; Fix, S. E.; Mascarella, S. W.; Vinson, N. A.; Xu, H.; Dersch, C. M.; Lu, Y.; Cantrell, B. E.; Zimmerman, D. M.; Carroll, F. I. Identification of the first trans-(3R,4R)-dimethyl-4-(3-hydroxyphenyl)piperidine derivative to possess highly potent and selective opioid kappa receptor antagonist activity. *J. Med. Chem.* **2001**, *44*, 2687−2690.

(21) Dror, R. O.; Pan, A. C.; Arlow, D. H.; Borhani, D. W.; Maragakis, P.; Shan, Y.; Xu, H.; Shaw, D. E. Pathway and mechanism of drug binding to G-protein-coupled receptors. *Proc. Natl. Acad. Sci. U. S. A.* **2011**, *108*, 13118−13123.

(22) Heifetz, A.; Morris, G. B.; Biggin, P. C.; Barker, O.; Fryatt, T.; Bentley, J.; Hallett, D.; Manikowski, D.; Pal, S.; Reifegerste, R.; Slack, M.; Law, R. Study of human Orexin-1 and -2 G-protein-coupled receptors with novel and published antagonists by modeling, molecular dynamics simulations, and site-directed mutagenesis. *Biochemistry* **2012**, *51*, 3178−3197.

(23) Provasi, D.; Artacho, M. C.; Negri, A.; Mobarec, J. C.; Filizola, M. Ligand-induced modulation of the free-energy landscape of G protein-coupled receptors explored by adaptive biasing techniques. *PLoS Comput. Biol.* **2011**, *7*, e1002193.

(24) Provasi, D.; Filizola, M. Putative active states of a prototypic g-protein-coupled receptor from biased molecular dynamics. *Biophys. J.* **2010**, *98*, 2347−2355.

(25) Provasi, D.; Bortolato, A.; Filizola, M. Exploring molecular mechanisms of ligand recognition by opioid receptors with metadynamics. *Biochemistry* **2009**, *48*, 10020−10029.

(26) Tosh, D. K.; Phan, K.; Gao, Z. G.; Gakh, A. A.; Xu, F.; Deflorian, F.; Abagyan, R.; Stevens, R. C.; Jacobson, K. A.; Katritch, V.

Optimization of adenosine 5′-carboxamide derivatives as adenosine receptor agonists using structure-based ligand design and fragment screening. *J. Med. Chem.* **2012**, *55*, 4297−4308.
(27) Deflorian, F.; Kumar, T. S.; Phan, K.; Gao, Z. G.; Xu, F.; Wu, H.; Katritch, V.; Stevens, R. C.; Jacobson, K. A. Evaluation of molecular modeling of agonist binding in light of the crystallographic structure of an agonist-bound A(2)A adenosine receptor. *J. Med. Chem.* **2012**, *55*, 538−552.
(28) McGovern, D. L.; Mosier, P. D.; Roth, B. L.; Westkaemper, R. B. CoMFA analyses of C-2 position salvinorin A analogs at the kappa-opioid receptor provides insights into epimer selectivity. *J. Mol. Graphics Modell.* **2010**, *28*, 612−625.
(29) Perez, D. M.; Karnik, S. S. Multiple signaling states of G-protein-coupled receptors. *Pharmacol Rev.* **2005**, *57*, 147−161.
(30) Graves, A. P.; Shivakumar, D. M.; Boyce, S. E.; Jacobson, M. P.; Case, D. A.; Shoichet, B. K. Rescoring docking hit lists for model cavity sites: predictions and experimental testing. *J. Mol. Biol.* **2008**, *377*, 914−934.
(31) Fiser, A.; Do, R. K.; Sali, A. Modeling of loops in protein structures. *Protein Sci.* **2000**, *9*, 1753−1773.
(32) Sali, A.; Blundell, T. L. Comparative protein modelling by satisfaction of spatial restraints. *J. Mol. Biol.* **1993**, *234*, 779−815.
(33) Krivov, G. G.; Shapovalov, M. V.; Dunbrack, R. L., Jr. Improved prediction of protein side-chain conformations with SCWRL4. *Proteins* **2009**, *77*, 778−795.
(34) Case, D. A.; Cheatham, T. E., 3rd; Darden, T.; Gohlke, H.; Luo, R.; Merz, K. M., Jr.; Onufriev, A.; Simmerling, C.; Wang, B.; Woods, R. J. The Amber biomolecular simulation programs. *J. Comput. Chem.* **2005**, *26*, 1668−1688.
(35) Case, D. A.; Darden, T. A.; Cheatham, T. E., III; Simmerling, C.; Wang, J.; Duke, R. E.; Luo, R.; Walker, R. C.; Zhang, W.; Merz, K. M.; Roberts, B. P.; Wang, B.; Hayik, S.; Roitberg, A.; Seabra, G.; Kolossvary, I.; Wong, K. F.; Paesani, F.; Vanicek, J.; Liu, J.; Wu, X.; Brozell, S. R.; Steinbrecher, T.; Gohlke, H.; Cai, Q.; Ye, X.; Wang, J.; Hsieh, M. J.; Cui, G.; Roe, D. R.; Mathews, D. H.; Seetin, M. G.; Sagui, C.; Babin, V.; Luchko, T.; Gusarov, S.; Kovalenko, A.; Kollman, P. A. *AMBER 11*; University of California: San Francisco, CA, 2010.
(36) Hooft, R. W.; Vriend, G.; Sander, C.; Abola, E. E. Errors in protein structures. *Nature* **1996**, *381*, 272.
(37) Vriend, G. WHAT IF: a molecular modeling and drug design program. *J. Mol. Graphics* **1990**, *8*, 52−56.
(38) Bas, D. C.; Rogers, D. M.; Jensen, J. H. Very fast prediction and rationalization of pKa values for protein-ligand complexes. *Proteins* **2008**, *73*, 765−783.
(39) Li, H.; Robertson, A. D.; Jensen, J. H. Very fast empirical prediction and rationalization of protein pKa values. *Proteins* **2005**, *61*, 704−721.
(40) Dolinsky, T. J.; Nielsen, J. E.; McCammon, J. A.; Baker, N. A. PDB2PQR: an automated pipeline for the setup of Poisson-Boltzmann electrostatics calculations. *Nucleic Acids Res.* **2004**, *32*, W665−W667.
(41) Katritch, V. Department of Integrative Structural and Computational Biology, The Scripps Research Institute, Personal communication, La Jolla, CA, May 2012.
(42) Hornak, V.; Abel, R.; Okur, A.; Strockbine, B.; Roitberg, A.; Simmerling, C. Comparison of multiple Amber force fields and development of improved protein backbone parameters. *Proteins* **2006**, *65*, 712−725.
(43) Pettersen, E. F.; Goddard, T. D.; Huang, C. C.; Couch, G. S.; Greenblatt, D. M.; Meng, E. C.; Ferrin, T. E. UCSF Chimera–a visualization system for exploratory research and analysis. *J. Comput. Chem.* **2004**, *25*, 1605−1612.
(44) Frisch, M. J.; Trucks, G. W.; Schlegel, H. B.; Scuseria, G. E.; Robb, M. A.; Cheeseman, J. R.; Scalmani, G.; Barone, V.; Mennucci, B.; Petersson, G. A.; Nakatsuji, H.; Caricato, M.; Li, X.; Hratchian, H. P.; Izmaylov, A. F.; Bloino, J.; Zheng, G.; Sonnenberg, J. L.; Hada, M.; Ehara, M.; Toyota, K.; Fukuda, R.; Hasegawa, J.; Ishida, M.; Nakajima, T.; Honda, Y.; Kitao, O.; Nakai, H.; Vreven, T.; Montgomery, J. A., Jr.; Peralta, J. E.; Ogliaro, F.; Bearpark, M.; Heyd, J. J.; Brothers, E.; Kudin, K. N.; Staroverov, V. N.; Kobayashi, R.; Normand, J.; Raghavachari, K.; Rendell, A.; Burant, J. C.; Iyengar, S. S.; Tomasi, J.; Cossi, M.; Rega, N.; Millam, J. M.; Klene, M.; Knox, J. E.; Cross, J. B.; Bakken, V.; Adamo, C.; Jaramillo, J.; Gomperts, R.; Stratmann, R. E.; Yazyev, O.; Austin, A. J.; Cammi, R.; Pomelli, C.; Ochterski, J. W.; Martin, R. L.; Morokuma, K.; Zakrzewski, V. G.; Voth, G. A.; Salvador, P.; Dannenberg, J. J.; Dapprich, S.; Daniels, A. D.; Farkas, Ö.; Foresman, J. B.; Ortiz, J. V.; Cioslowski, J.; Fox, D. J. In *Revision A*; Gaussian, Inc.: Wallingford, CT, 2009.
(45) Wang, J.; Wolf, R. M.; Caldwell, J. W.; Kollman, P. A.; Case, D. A. Development and testing of a general amber force field. *J. Comput. Chem.* **2004**, *25*, 1157−1174.
(46) Jorgensen, W. L.; Chandrasekhar, J.; Madura, J. D.; Impey, R. W.; Klein, M. L. Comparison of Simple Potential Functions for Simulating Liquid Water. *J. Chem. Phys.* **1983**, *79*, 926−935.
(47) Darden, T.; York, D.; Pedersen, L. Particle mesh Ewald: An N·log(N) method for Ewald sums in large systems. *J. Chem. Phys.* **1993**, *98*, 10089−10092.
(48) Ryckaert, J. P.; Ciccotti, G.; Berendsen, H. J. C. Numerical integration of the Cartesian Equations of Motion of a System with Constraints: Molecular Dynamics of n-Alkanes. *J. Comput. Phys.* **1977**, *23*, 327−341.
(49) Izaguirre, J. A.; Catarello, D. P.; Wozniak, J. M.; Skeel, R. D. Langevin stabilization of molecular dynamics. *J. Chem. Phys.* **2001**, *114*, 2090−2098.
(50) Simmerling, C.; Elber, R.; Zhang, J. Moil-view-A program for visualization of structure and dynamics of biomolecules and STO-A program for computing stochastic paths. The Jerusalem Symposia on Quantum Chemistry and Biochemistry, *Modelling of Biomolecular Structures and Mechanisms*, Pullman, A., Jortner, J., Eds.; Springer: Jerusalem, Israel, 1995; Vol. *27*, pp 241−265.
(51) Phillips, J. C.; Braun, R.; Wang, W.; Gumbart, J.; Tajkhorshid, E.; Villa, E.; Chipot, C.; Skeel, R. D.; Kale, L.; Schulten, K. Scalable molecular dynamics with NAMD. *J. Comput. Chem.* **2005**, *26*, 1781−1802.
(52) Kollman, P. A.; Massova, I.; Reyes, C.; Kuhn, B.; Huo, S.; Chong, L.; Lee, M.; Lee, T.; Duan, Y.; Wang, W.; Donini, O.; Cieplak, P.; Srinivasan, J.; Case, D. A.; Cheatham, T. E., 3rd Calculating structures and free energies of complex molecules: combining molecular mechanics and continuum models. *Acc. Chem. Res.* **2000**, *33*, 889−897.
(53) Gohlke, H.; Kiel, C.; Case, D. A. Insights into protein-protein binding by binding free energy calculation and free energy decomposition for the Ras-Raf and Ras-RalGDS complexes. *J. Mol. Biol.* **2003**, *330*, 891−913.
(54) Wang, W.; Kollman, P. A. Computational study of protein specificity: the molecular basis of HIV-1 protease drug resistance. *Proc. Natl. Acad. Sci. U. S. A.* **2001**, *98*, 14937−14942.
(55) Xu, Y.; Wang, R. A computational analysis of the binding affinities of FKBP12 inhibitors using the MM-PB/SA method. *Proteins* **2006**, *64*, 1058−1068.
(56) Honig, B.; Nicholls, A. Classical electrostatics in biology and chemistry. *Science* **1995**, *268*, 1144−1149.
(57) Weiser, J.; Shenkin, P. S.; Still, W. C. Approximate atomic surfaces from linear combinations of pairwise overlaps (LCPO). *J. Comput. Chem.* **1999**, *20*, 217−230.
(58) Hou, T.; Wang, J.; Li, Y.; Wang, W. Assessing the performance of the MM/PBSA and MM/GBSA methods. 1. The accuracy of binding free energy calculations based on molecular dynamics simulations. *J. Chem. Inf. Model.* **2011**, *51*, 69−82.
(59) Miller, B. R., 3rd; McGee, T. D., Jr.; Swails, J. M.; Homeyer, N.; Gohlke, H.; Roitberg, A. E. MMPBSA.py: An Efficient Program for End-State Free Energy Calculations. *J. Chem. Theory Comput.* **2012**, *8*, 3314−3321.
(60) Su, P.; Li, H. Energy decomposition analysis of covalent bonds and intermolecular interactions. *J. Chem. Phys.* **2009**, *131*, 014102.
(61) Boys, S. F.; Bernardi, F. Calculation of Small Molecular Interactions by Differences of Separate Total Energies - Some Procedures with Reduced Errors. *Mol. Phys.* **1970**, *19*, 553−566.

(62) Schmidt, M. W.; Baldridge, K. K.; Boatz, J. A.; Elbert, S. T.; Gordon, M. S.; Jensen, J. H.; Koseki, S.; Matsunaga, N.; Nguyen, K. A.; Su, S. J.; Windus, T. L.; Dupuis, M.; Montgomery, J. A. General Atomic and Molecular Electronic-Structure System. *J. Comput. Chem.* **1993**, *14*, 1347−1363.
(63) Bader, R. F. W. *Atoms in Molecules: A Quantum Theory*; Clarendon: Oxford: 1990.
(64) Bader, R. F. W. A bond path: A universal indicator of bonded interactions. *J. Phys. Chem. A* **1998**, *102*, 7314−7323.
(65) Grabowski, S. J. Hydrogen bonding strength - measures based on geometric and topological parameters. *J. Phys. Org. Chem.* **2004**, *17*, 18−31.
(66) Espinosa, E.; Molins, E.; Lecomte, C. Hydrogen bond strengths revealed by topological analyses of experimentally observed electron densities. *Chem. Phys. Lett.* **1998**, *285*, 170−173.
(67) Biegler-Konig, F.; Schonbohm, J. Update of the AIM2000-program for atoms in molecules. *J. Comput. Chem.* **2002**, *23*, 1489−1494.
(68) Collu, F.; Ceccarelli, M.; Ruggerone, P. Exploring binding properties of agonists interacting with a delta-opioid receptor. *PLoS One* **2012**, *7*, e52633.
(69) Kukic, P.; Nielsen, J. E. Electrostatics in proteins and protein-ligand complexes. *Future Med. Chem.* **2010**, *2*, 647−666.
(70) Leonis, G.; Steinbrecher, T.; Papadopoulos, M. G. A contribution to the drug resistance mechanism of darunavir, amprenavir, indinavir, and saquinavir complexes with HIV-1 protease due to flap mutation I50V: a systematic MM-PBSA and thermodynamic integration study. *J. Chem. Inf. Model.* **2013**, *53*, 2141−2153.
(71) Politi, A.; Leonis, G.; Tzoupis, H.; Ntountaniotis, D.; Papadopoulos, M. G.; Grdadolnik, S. G.; Mavromoustakos, T. Conformational Properties and Energetic Analysis of Aliskiren in Solution and Receptor Site. *Mol. Inf.* **2011**, *30*, 973−985.
(72) Tzoupis, H.; Leonis, G.; Durdagi, S.; Mouchlis, V.; Mavromoustakos, T.; Papadopoulos, M. G. Binding of novel fullerene inhibitors to HIV-1 protease: insight through molecular dynamics and molecular mechanics Poisson-Boltzmann surface area calculations. *J. Comput.-Aided Mol. Des* **2011**, *25*, 959−976.
(73) Tzoupis, H.; Leonis, G.; Megariotis, G.; Supuran, C. T.; Mavromoustakos, T.; Papadopoulos, M. G. Dual inhibitors for aspartic proteases HIV-1 PR and renin: advancements in AIDS-hypertension-diabetes linkage via molecular dynamics, inhibition assays, and binding free energy calculations. *J. Med. Chem.* **2012**, *55*, 5784−5796.
(74) Gouda, H.; Kuntz, I. D.; Case, D. A.; Kollman, P. A. Free energy calculations for theophylline binding to an RNA aptamer: Comparison of MM-PBSA and thermodynamic integration methods. *Biopolymers* **2003**, *68*, 16−34.
(75) Runyon, S. P.; Brieaddy, L. E.; Mascarella, S. W.; Thomas, J. B.; Navarro, H. A.; Howard, J. L.; Pollard, G. T.; Carroll, F. I. Analogues of (3R)-7-hydroxy-N-[(1S)-1-{[(3R,4R)-4-(3-hydroxyphenyl)-3,4-dimethyl-1-piperidinyl]methyl}-2-methylpropyl)-1,2,3,4-tetrahydro-3-isoquinolinecarboxamide (JDTic). Synthesis and in vitro and in vivo opioid receptor antagonist activity. *J. Med. Chem.* **2010**, *53*, 5290−5301.
(76) Kane, B. E.; Nieto, M. J.; McCurdy, C. R.; Ferguson, D. M. A unique binding epitope for salvinorin A, a non-nitrogenous kappa opioid receptor agonist. *FEBS J.* **2006**, *273*, 1966−1974.
(77) Vortherms, T. A.; Mosier, P. D.; Westkaemper, R. B.; Roth, B. L. Differential helical orientations among related G protein-coupled receptors provide a novel mechanism for selectivity. Studies with salvinorin A and the kappa-opioid receptor. *J. Biol. Chem.* **2007**, *282*, 3146−3156.
(78) Yan, F.; Mosier, P. D.; Westkaemper, R. B.; Roth, B. L. Galpha-subunits differentially alter the conformation and agonist affinity of kappa-opioid receptors. *Biochemistry* **2008**, *47*, 1567−1578.
(79) Yan, F.; Mosier, P. D.; Westkaemper, R. B.; Stewart, J.; Zjawiony, J. K.; Vortherms, T. A.; Sheffler, D. J.; Roth, B. L. Identification of the molecular mechanisms by which the diterpenoid salvinorin A binds to kappa-opioid receptors. *Biochemistry* **2005**, *44*, 8643−8651.
(80) Jo, S.; Kim, T.; Iyer, V. G.; Im, W. CHARMM-GUI: a web-based graphical user interface for CHARMM. *J. Comput. Chem.* **2008**, *29*, 1859−1865.
(81) Jo, S.; Lim, J. B.; Klauda, J. B.; Im, W. CHARMM-GUI Membrane Builder for mixed bilayers and its application to yeast membranes. *Biophys. J.* **2009**, *97*, 50−58.
(82) Orientations of Proteins in Membranes (OPM) database. http://opm.phar.umich.edu (accessed June 27, 2014).